

GSA DATA REPOSITORY 2020148**Hematite (U-Th)/He thermochronometry detects asperity flash heating during laboratory earthquakes****Gabriele Calzolari¹, Alexis K. Ault¹, Greg Hirth², and Robert G. McDermott¹**¹*Utah State University, Department of Geosciences, Logan, UT 84322*²*Brown University, Department of Earth, Environmental and Planetary Sciences, Providence, RI 02912***1. Starting material textural characterization, grain size analysis, and closure temperature calculations**

Secondary electron images of representative hematite aliquots of starting material were acquired on a Quanta 650 FEG scanning electron microscope (SEM) housed in Utah State University's Microscopy Core Facility. Samples were prepared for imaging by mounting representative aliquots in epoxy in a 1" plastic ring form and hand polished to 1 μm using diamond polishing papers and sonication in between polishing steps. Secondary electron imaging was conducted in low vacuum-variable pressure mode at 0.5-0.8 Torr, with 16-20 kV, and 8.5-11.4 mm working distance. Images were acquired at various scales such that images at the smallest field of view are a component of the larger field of view.

The thickness (diameter) of individual plates ($n = 693$) in the undeformed specularite (polycrystalline aggregates of specular hematite) and isolated single plates of starting material ($n = 16$) were measured using ImageJ software. Corresponding hematite (U-Th)/He (He) closure temperatures (T_c) were calculated assuming correspondence of observable plate half-width to diffusion domain length scale (Evenson et al., 2014; Jensen et al., 2018), hematite He diffusion kinetics of Farley (2018), and a 10 $^{\circ}\text{C}/\text{Ma}$ cooling rate. The measured hematite plate widths for individual plates with corresponding calculated T_c are presented in Table DR1.

2. Experimental set up and sample preparation

Deformation experiments were conducted on specimens prepared from an ~ 30 cm-diameter specular hematite boulder, retrieved from the central Wellsville Mountains, UT, USA (41.560278° , -111.990278°). The boulder was cut into 1.5-2 cm thick slabs using a water-cooled rock saw and adjacent slabs were used for experiments reported here. Frictional sliding experiments on specular hematite were performed in an Instron 1 atm rotary shear apparatus at

ambient temperature and humidity at the Experimental Rock Mechanics lab at Brown University. Experiments were conducted by sliding a SiC ring against a fixed specular hematite slab (Fig. DR1). The SiC ring (4.77 mm wide with a 22.2 mm inner radius) was prepared from a commercially available sharpening stone (Norton Combination India Stone Item # NCMBN11x2). Prior to the sliding tests, hematite slabs were surface-ground in water to prevent He loss (i.e., thermal resetting), and then roughened with 100# SiC grit in water on a glass plate. Data including torque, normal force, normal displacement, and angular displacement were acquired at sampling rates up to 5 kHz. Two types of experiments were performed: “continuous slip” and “interrupted slip.” Additional details of the experimental conditions for each experiment type are provided in the main text and data outputs are shown in figures DR2, DR3, and DR4.

3. Sample preparation for hematite (U-Th)/He analyses of starting material and run products

Hematite sampling and aliquot selection for (U-Th)/He dating was carried out at the Utah State University Mineral Microscopy and Separation Lab.

A. Undeformed

(1) *Single plates:* Hundreds of individual hematite plates of undeformed hematite (starting material) were extracted from the specularite boulder to determine the range in plate thickness. Single plates were mounted on double-sided copper sticky tape and imaged using SEM secondary (SE) microscopy. The thickness of the individual plates was measured using ImageJ software and T_c was determined following the approach described above. Single plates encompassing the range of observed plate thicknesses (T_c) were then hand-picked from the sticky tape and packed in Nb tubes for He, U, and Th measurements.

(2) *Homogenized:* The positive date-plate thickness relationship with hematite He dates reflects the grain size (plate thickness) control on He diffusion and the post-mineralization thermal history. Owing to relationship, it was necessary to “homogenize” the grain size our undeformed material to create a benchmark (U-Th)/He date for comparison with deformation run products. These aliquots were prepared by crushing 2 cm³ aliquots extracted from of the margin of each hematite slab that was used in a deformation experiment. Crushing was done by hand in ethanol using mortar and pestle to obtain a homogenous powder with particles >50 μm in diameter. The

homogenized material was then pipetted into Nb tubes, which were carefully pinched shut at both ends so that ultra-fine-grained material was not lost. A total of six homogenized aliquots, three from each hematite slab of the continuous slip and the interrupted slip experiments were prepared for (U-Th)/He dating.

B. Experimental run products

Two types of aliquots were retrieved from the experimentally-produced fault surfaces following deformation experiments: fault gouge and fault mirror (FM) material (see main text and Fig. 2 for descriptions of each). Delicate FM material and gouge material were carefully lifted from the fault surface using a razor blade and transferred to separate petri dishes. The number of aliquots analyzed was limited by the ability to exclusively sample the target material (vs. the underlying undeformed and coarser-grained specular hematite) and by the extremely fissile and thus fragile nature of the run products. The material was then carefully pipetted out in ethanol and transferred into Nb tubes under a stereoscope. Nb tubes were carefully pinched shut at each end using tweezers to contain the ultra-fine material within them. Three gouge and three FM aliquots were prepared for hematite (U-Th)/He analysis from both types of experiment.

4. Hematite (U-Th)/He dating

Hematite aliquots were analyzed for He, U, and Th at the University of Arizona Noble Gas Laboratory. The previously selected and packed hematite aliquots were heated to temperatures ~975-1065 °C and associated packet “low glow” comparable to temperatures for apatite lasing. Aliquots were lased for ~8-10 minutes using a diode laser in an ultra-high vacuum gas extraction line. Extracted He gas was spiked with ^3He , purified using cryogenic and gettering methods, and analyzed on a quadrupole mass spectrometer. Each aliquot was heated a second time to temperatures slightly greater than the first extraction until negligible gas was released. The majority of samples required one and a few required two re-extractions to extract all He. Analysis of a known quantity of ^4He was performed after every 4-5 unknown analyses to monitor instrumental sensitivity drift. U and Th contents of each aliquot were measured by isotope dilution and solution ICPMS. The degassed packets were dissolved in hydrochloric acid in a pressure digestion vessel (Parr bomb). Following addition of a ^{233}U - ^{229}Th spike, equilibration, and dissolution, U and Th isotopes were measured on an Element 2 ICP-MS. Hematite from sample

WF94-17 was used as an internal lab standard to monitor chemistry analyses and analyzed by the same procedures with the batch of unknowns.

We do not apply an alpha-ejection correction to our hematite He dates because the aliquots, derived from a slab are part of a larger initial sample (i.e., the boulder) with dimensions significantly larger than the alpha-stopping distance. In addition, hematite slip surfaces are localized in gouge and there is gouge on the upper SiC ring. Both of these observations support that alpha ejection is balanced by implantation. Hematite dates were determined assuming that the grains were unzoned in U and Th. Detailed (U-Th)/He analytical results are reported in Table DR2.

Analyses to evaluate anomalous Th/U ratios: We also analyzed an additional suite of undegassed homogenized material aliquots for their U and Th contents to evaluate relationships between elevated Th/U ratios and anomalously old or young dates. *Undegassed homogenized aliquots yield overlapping Th/U ratios with most aliquots heated with the diode laser*, such as single plate aliquots, homogenized material from slabs of each experiment, and FM and gouge aliquots for the continuous and interrupted slip experiments (Table DR2).

(1) One undeformed single plate aliquot (EXP_2_H6) and one FM aliquot (22_S_H2) have high Th/U ratios, low U, and old (U-Th)/He dates relative to all other analyzed starting material including undegassed aliquots. The combination of these observations suggest these aliquots experienced U volatilization during lasing and He extraction, described in (2013).

(2) Undeformed single plate aliquot EXP_2_H3 yields a (U-Th)/He date that is consistent with the observed range of dates from all starting material aliquots. However, this aliquot yields anomalously low U content, elevated Th/U ratio, and its date deviates from the date-plate thickness (grain size) trend characterized by all other single plate aliquots, which questions the veracity of this analysis.

(3) FM aliquot 23_S_H3 exhibits an elevated Th/U ratio compared to degassed and undegassed starting material values as well as a young (U-Th)/He date relative to the other aliquots of this type. This combination may reflect Th addition from breakdown of the upper SiC ring during the experiment.

In summary, we exclude two single plate aliquots and two FM aliquots, one each from the continuous slip and interrupted slip experiments, from He loss calculations and discussion. We note that both FM aliquots exhibit anomalous Th/U ratios much higher than their corresponding undeformed homogenized aliquot values, the single plates of starting material, and the undegassed

aliquots (Fig. DR8). We emphasize that Th/U ratios from the remainder of the run products overlap with corresponding homogenized material, single plates, and undegassed aliquot Th/U values, supporting the robustness of these data.

5. Temperature rise and hematite He loss calculations

A. Hematite He loss assessment

To quantify He loss from hematite on experimental fault surfaces, we apply a first-order approximation of the (U-Th)/He age equation:

$$t \approx \frac{[{}^4\text{He}]}{\{8\lambda_{238} [{}^{238}\text{U}] + 7\lambda_{235} [{}^{235}\text{U}] + 6\lambda_{232} [{}^{232}\text{Th}]\}} \quad (1)$$

Where t is time, λ is the decay constant, and [He, U, Th] are measured concentrations of He, U, and Th. Because $t \propto [{}^4\text{He}]$, we can directly compare the difference between mean dates for the homogenized starting material and the dates from aliquots of FM and gouge from corresponding hematite slabs, and then calculate the faulting-induced He loss for each aliquot. We therefore calculate %He loss:

$$\%He \text{ loss} = \frac{(H_{md} - RP_{iad}) * 100}{H_{md}} \quad (2)$$

where H_{md} is the mean date for the undeformed homogenized material and RP_{iad} is the individual aliquot date for the run products. Calculation results are reported in Table DR3.

B. Friction-generated heat calculations

During faulting at seismic slip velocities (>0.1 m/s), heat production outpaces heat dissipation and shear heating at the slip surface may be high (e.g., Lachenbruch, 1986). To assess the frictional-generated heat in a fault, we consider the bulk fault temperature rise and temperatures generated at frictional contacts, referred to as asperity flash heating (AFH). The former describes the temperature rise experienced by the fault volume during and after a certain slip displacement, and the latter describes the short-lived ($\ll 1$ s) temperature rise on a single micro asperity ($\ll 1$ mm in diameter).

To calculate the average fault surface temperature (*ASFT*) achieved during our experiments, we use the equation Lachenbruch (1986):

$$AFST = T_{amb} + \frac{\mu\sigma_n}{\rho c} * \frac{V\sqrt{t}}{\sqrt{\pi\alpha}} \quad (3)$$

where T_{amb} is the ambient temperature, μ is the coefficient of friction, σ_n is the normal stress, ρ is density, c is heat capacity, V is slip velocity, t is the duration of slip, and α is thermal diffusivity.

The maximum attainable *temperature at a circular frictional contact*, commonly defined as T_{fc} but here as AFH for consistency, is (Archard, 1959):

$$AFH \approx AFST + \left(\frac{\pi H \mu V a}{8 \rho c \alpha} \beta \right) \quad \text{for } Pe < 5 \quad (4)$$

where $AFST$ is defined by equation (3), H is the indentation hardness of the mineral, and a is the asperity radius. Pe refers to the Peclet number, or the ratio of the timescales of advection of the heat source to conduction and defined as $Pe = Va / 2\alpha$. The factor β is a coefficient that describes heat partitioning between two opposing bodies in contact. β is a function of Pe and can be estimated numerically or graphically, although readily available graphical solutions are for non-circular contacts (e.g., Jaeger, 1942; Archard, 1959). For ease of implementation, we take previously reported tabular values for β given by Archard (1959) and apply a linear interpolation between them such that β is ~ 1 for $Pe \leq 0.1$, and on the order of 0.5 for $Pe = 5$. We thus assume:

$$\beta \approx 1 - 0.1Pe \quad (5)$$

We report parameters used for calculating $AFST$ and AFH in Table DR4. Calculation results are reported for a range of asperity diameters in Figure 4 of the main text. Finally, we calculate the duration of the heat pulse generated by an asperity, AFH , using the asperity lifetime (i.e., $AFH = 2a/V$). Calculated $AFST$ and AFH values shown in Figure 4 are also reported in Table DR5.

C. Assessing temperature and time responsible for the observed He loss

Fractional He loss in the hematite (U-Th)/He system is governed by three variables: temperature, time or hold time for which such temperature is maintained, and the radius of the diffusion domain (here approximated by hematite plate thickness half-width or nanoparticle radius). To assess the range of the magnitude and duration of the friction-generated heat responsible for the observed He loss, we consider the simplified and rearranged equation for fractional He loss:

$$\ln(t) = \ln \left\{ \left[\frac{1}{\pi^2} - \frac{\left(\frac{9}{\pi - 3f} \right)^{\frac{1}{2}}}{3} \right]^2 \frac{a^2}{D_0} \right\} + \frac{E_a}{R} \left(\frac{1}{T} \right) \quad (6)$$

where f is He fractional loss, a is the radius of the diffusion domain (plate thickness half-width), D_0 is the frequency factor, E_a is the activation energy, R is the gas constant, and T is temperature (McDougall et al., 1999; Reiners et al., 2007). Using secondary electron images of the experimentally-produced fault surfaces, we measure the grain-size populations for FMs and gouge from continuous and interrupted slip experiments (Fig. DR7). Using equation (3), we then calculate the fractional He loss contours (in terms of T and t) for each experiment and for the measured maximum and minimum grain size from the FM zones (Fig. DR8), assuming a square-pulse heating event and hematite He diffusion parameters of Farley (2018).

REFERENCES

- Archard, J.F., 1959, The temperature of rubbing surfaces: *Wear*, v. 2, p. 438-455.
- Chase, M., 1983, Heats of Transition of the Elements: *Bull. Alloy Phase Diagrams*, v. 4, p. 124-124.
- Chicot, D., Mendoza, J., Zaoui, A., Louis, G., Lepingle, V., Roudet, F., and Lesage, J., 2011, Mechanical properties of magnetite (Fe₃O₄), hematite (α-Fe₂O₃) and goethite (α-FeO·OH) by instrumented indentation and molecular dynamics analysis: *Materials Chemistry and Physics*, v. 129, p. 862-870.
- Evenson, N.S., Reiners, P.W., Spencer, J.E., and Shuster, D.L., 2014, Hematite and mn oxide (U-Th)/He dates from the buckskin-Rawhide detachment system, Western Arizona: Gaining insights into hematite (U-Th)/He systematics: *American Journal of Science*, v. 314, p. 1373-1435.
- Farley, K.A., 2018, Helium diffusion parameters of hematite from a single-diffusion-domain crystal: *Geochimica et Cosmochimica Acta*, v. 231, p. 117-129.
- Horai, K., 1971, Thermal conductivity of rock-forming minerals: *Journal of Geophysical Research*, v. 76, p. 1278-1308.
- Jaeger, J., 1942, Moving heat sources and friction temperature, *Proc. Roy. Soc. NSW*, Volume 76, p. 203-224.
- Jensen, J.L., Siddoway, C.S., Reiners, P.W., Ault, A.K., Thomson, S.N., and Steele-MacInnis, M., 2018, Single-crystal hematite (U-Th)/He dates and fluid inclusions document widespread Cryogenian sand injection in crystalline basement: *Earth and Planetary Science Letters*, v. 500, p. 145-155.
- Kohli, A.H., Goldsby, D.L., Hirth, G., and Tullis, T., 2011, Flash weakening of serpentinite at near-seismic slip rates: *Journal of Geophysical Research: Solid Earth*, v. 116.
- Lachenbruch, A.H., 1986, Simple models for the estimation and measurement of frictional heating by an earthquake, Open-File Report.
- McDougall, I., Mac Dougall, I., and Harrison, T.M., 1999, *Geochronology and Thermochronology by the 40Ar/39Ar Method*, Oxford University Press on Demand.
- Nesse, W.D., 2012, *Introduction to mineralogy*.
- Reiners, P.W., Thomson, S.N., McPhillips, D., Donelick, R.A., and Roering, J.J., 2007, Wildfire thermochronology and the fate and transport of apatite in hillslope and fluvial environments: *Journal of Geophysical Research: Earth Surface*, v. 112.

- Rowe, C.D., and Griffith, W.A., 2015, Do faults preserve a record of seismic slip: A second opinion: *Journal of Structural Geology*, v. 78, p. 1-26.
- Vasconcelos, P.M., Heim, J.A., Farley, K.A., Monteiro, H., and Waltenberg, K., 2013, $^{40}\text{Ar}/^{39}\text{Ar}$ and (U-Th)/He - $^4\text{He}/^3\text{He}$ geochronology of landscape evolution and channel iron deposit genesis at Lynn Peak, Western Australia: *Geochimica et Cosmochimica Acta*, v. 117, p. 283-312.

DATA**Table DR1: Hematite plate thickness measurements and closure temperature estimates**

plate thickness (μm)	T _c (°C)								
30.0	165	34.0	164	26.7	159	6.7	137	9.0	141
27.4	160	28.6	161	17.0	152	29.9	162	14.5	149
100.0	184	11.0	144	13.3	148	84.6	181	9.9	143
13.5	148	10.1	143	6.6	136	17.9	153	7.0	137
18.3	153	20.9	155	9.4	142	9.6	142	9.8	143
18.3	153	25.3	159	3.7	128	131.2	189	6.9	137
19.1	154	26.6	159	9.6	142	197.5	197	8.3	140
31.0	162	14.2	149	1.9	117	32.8	163	10.7	144
13.6	148	28.0	160	2.2	120	60.4	174	10.0	143
15.4	150	19.1	154	5.3	133	49.2	170	14.9	150
24.1	158	17.1	152	3.6	127	88.1	181	13.1	147
26.6	159	12.4	147	3.5	127	9.3	142	16.3	151
20.1	155	52.4	172	2.4	121	21.1	155	17.4	152
20.5	155	23.1	157	2.0	118	15.0	150	10.6	144
16.7	151	18.5	153	1.7	116	22.2	156	41.3	167
11.8	146	10.0	143	1.7	116	7.6	139	30.0	162
13.8	148	10.0	143	3.5	127	8.6	141	13.8	148
5.6	134	12.9	147	5.8	134	5.4	133	25.3	159
13.3	148	30.9	162	3.8	128	13.7	148	34.0	164
25.4	159	11.9	146	14.8	149	4.8	132	13.1	147
7.5	138	12.4	147	11.2	145	5.7	134	15.0	150
15.8	151	11.1	145	13.3	148	4.6	131	26.7	159
21.1	155	14.1	149	6.4	136	26.7	160	15.6	150
28.3	161	11.8	146	8.9	141	21.8	156	21.3	156
40.5	167	16.1	151	28.9	161	16.6	151	26.7	160
23.4	157	23.4	157	4.5	130	16.3	151	6.1	135
13.0	147	10.1	143	5.3	133	39.7	167	29.0	161
18.9	154	14.6	149	5.1	132	7.9	139	25.8	159
21.6	156	8.1	140	7.7	139	42.7	168	21.7	156
28.8	161	25.6	159	7.9	139	9.9	143	20.4	155
43.0	168	38.6	166	6.6	136	14.6	149	31.3	162
21.3	156	33.1	163	9.5	142	24.5	158	17.6	152
103.7	185	39.3	166	11.0	145	9.6	142	64.1	175
58.8	174	13.1	147	13.1	147	7.6	139	15.9	151
15.9	151	10.2	143	8.9	141	5.4	133	8.7	141
11.8	146	18.3	153	8.7	141	6.3	136	49.8	171
10.7	144	18.3	153	6.0	135	11.8	146	84.2	181
17.8	153	5.3	133	40.9	167	8.7	141	19.2	154
14.2	149	9.4	142	9.3	142	2.7	123	15.3	150
14.5	149	4.6	131	3.3	126	3.2	126	19.4	154
12.4	146	15.0	150	11.0	145	19.5	154	9.5	142
15.2	150	8.3	140	7.7	139	10.4	144	9.9	143
16.5	151	11.0	145	6.7	137	9.5	142	12.3	146
14.3	149	10.2	143	31.2	162	3.0	124	11.2	145
12.5	147	4.3	130	4.6	131	13.5	148	36.9	165
27.0	160	10.4	144	9.1	141	13.6	148	6.8	137

38.9	166	35.6	165	9.2	142	22.3	156	9.3	142
8.1	140	26.6	159	10.4	144	18.2	153	5.4	133
8.4	140	34.8	164	22.8	157	153.0	192	38.8	166
43.9	168	38.6	166	33.4	163	12.3	146	44.4	169
9.4	142	26.4	159	15.8	151	11.6	145	10.0	143
14.4	149	24.5	158	18.3	153	13.2	148	8.3	140
1.6	115	14.3	149	4.8	131	15.8	151	18.2	153
3.1	125	13.3	148	22.2	156	9.7	143	153.0	192
17.4	152	5.3	133	30.6	162	7.6	139	12.3	146
9.7	143	10.0	143	44.1	168	10.3	143	11.6	145
12.0	146	16.4	151	37.1	165	12.8	147	13.2	148
7.9	139	53.9	172	30.9	162	3.8	128	15.8	151
11.4	145	36.6	165	44.6	169	8.9	141	9.7	143
2.6	122	15.1	150	10.7	144	8.4	140	7.6	139
9.0	141	7.7	139	5.8	134	4.1	129	10.3	143
8.1	140	12.2	146	8.8	141	12.5	147	12.8	147
11.5	145	23.0	157	22.9	157	9.5	142	3.8	128
3.6	127	29.9	162	5.4	133	18.5	153	8.9	141
7.6	139	55.0	173	6.8	137	5.7	134	8.4	140
21.7	156	17.4	152	4.0	129	5.7	134	4.1	129
20.5	155	7.1	137	7.0	137	10.6	144	12.5	147
21.4	156	3.6	127	15.5	150	14.8	149	9.5	142
35.0	164	49.9	171	7.4	138	7.1	137	18.5	153
26.3	159	8.6	141	8.4	140	26.0	159	5.7	134
13.1	147	14.8	149	12.5	147	13.0	147	5.7	134
35.1	164	5.2	133	21.5	156	13.8	148	10.6	144
18.4	153	9.8	143	52.8	172	22.8	157	14.8	149
9.3	142	10.1	143	6.3	136	6.4	136	7.1	137
8.4	140	10.6	144	3.9	128	7.1	137	26.0	159
18.0	153	7.5	138	5.0	132	6.3	136	13.0	147
3.6	127	12.8	147	7.9	139	6.8	137	13.8	148
12.7	147	9.8	143	30.1	162	18.8	153	22.8	157
22.6	157	9.2	142	5.5	134	16.3	151	6.4	136
6.6	136	96.3	183	24.3	158	12.2	146	7.1	137
12.3	146	29.0	161	56.2	173	23.2	157	6.3	136
13.7	148	6.3	136	171.6	195	18.4	153	6.8	137
9.7	143	32.7	163	77.7	179	28.4	161	18.8	153
16.8	152	27.0	160	8.9	141	17.0	152	16.3	151
29.8	161	17.3	152	9.4	142	34.7	164	12.2	146
10.2	143	7.6	139	6.9	137	56.2	173	23.2	157
27.2	160	33.9	164	7.4	138	171.6	195	18.4	153
29.5	161	12.4	147	12.1	146	77.7	179	28.4	161
17.6	152	16.9	152	5.7	134	8.9	141	17.0	152
9.9	143	11.6	145	7.0	137	9.4	142	34.7	164
20.9	155	18.2	153	8.1	140	6.9	137	26.5	159
21.8	156	15.8	151	7.8	139	7.4	138	13.8	148
20.7	155	38.9	166	47.4	170	12.1	146	17.7	152
19.5	154	14.2	149	7.9	139	5.7	134	13.8	148
26.3	159	15.6	150	5.4	133	7.0	137	8.3	140
23.9	158	8.8	141	38.8	166	8.1	140	21.6	156
15.3	150	38.0	166	44.4	169	7.8	139	12.8	147
13.3	148	37.8	166	10.0	143	47.4	170	16.1	151
30.6	162	15.2	150	8.3	140	7.9	139	17.3	152
3.1	125	17.3	152	16.7	151	4.4	130	6.0	135

9.9	143	6.4	136	4.5	130	7.2	138	5.7	134
4.3	130	16.8	152	8.2	140	5.0	132	7.7	139
6.3	136	13.7	148	11.0	145	15.0	150	8.4	140
6.0	135	11.7	146	7.5	138	5.7	134	34.7	164
9.7	142	16.7	151	5.7	134	14.1	149	8.0	139
15.7	150	27.1	160	16.8	152	10.8	144	13.5	148
11.6	145	17.6	152	8.9	141	13.1	147	19.6	154
41.1	167	9.6	142	10.3	143	5.7	134	19.6	154
12.6	147	12.3	146	7.0	137	10.3	144	11.6	145
4.5	131	14.4	149	6.3	136	20.8	155	10.7	144
6.9	137	13.0	147	3.1	125	6.0	135	14.6	149
9.1	141	11.1	145	15.4	150	10.5	144	68.4	177
4.1	129	28.3	161	6.6	136	63.5	175	100.2	184
8.9	141	23.0	157	6.4	136	13.2	148	12.5	147
6.2	135	16.1	151	7.7	139	21.2	155	54.4	172
4.3	130	11.3	145	7.3	138	12.7	147	11.5	145
4.9	132	2.0	119	15.9	151	5.4	133	63.9	175
4.6	131	3.3	126	10.5	144	12.6	147	18.3	153
5.5	134	10.3	143	9.3	142	10.2	143	15.5	150
10.5	144	3.5	127	7.8	139	12.1	146	11.3	145
2.8	123	5.8	134	7.3	138	14.1	149	15.2	150
31.7	163	1.5	114	6.6	136	6.0	135	14.6	149
8.9	141	36.1	165	6.0	135	7.8	139	12.2	146
15.2	150	7.3	138	8.7	141	6.0	135	5.6	134
8.9	141	10.7	144	8.8	141	5.0	132	4.6	131
14.2	149	6.5	136	13.5	148	7.9	139	5.9	135
6.2	136	5.5	134	7.1	137	4.9	132	3.3	126
7.3	138	14.7	149	10.0	143	5.3	133	4.0	129
9.5	142	9.2	142	10.0	143	8.3	140	3.1	125
3.4	126	20.0	155	17.7	152	11.5	145	4.4	130
9.8	143	4.7	131	8.4	140	12.6	147	9.6	142
4.6	131	5.4	133	25.1	158	4.2	129	15.4	150
6.1	135	5.4	133	15.8	151	4.0	129	9.5	142
8.9	141	6.4	136	11.0	145	2.5	122	6.4	136
9.1	142	15.5	150	19.6	154	9.1	142	23.8	158
11.6	145	11.7	146	9.3	142	11.0	145	5.7	134
32.0	163	11.3	145	6.6	136	4.0	128	12.7	147
6.0	135	3.7	127	5.1	132	12.0	146	11.7	146
9.9	143	8.5	140	17.9	153				

Statistics

	plate thickness (μm)	T_c ($^{\circ}\text{C}$)
Mean	17	147
Max	197	197
Min	1	114
SD	20	13
max-min	196	83
Count	693	693

Table DR2: Hematite (U-Th)/He Thermochronometric Data

sample	He (pmol)	1 σ \pm He (pmol)	U (ng)	1 σ \pm U (ng)	Th (ng)	1 σ \pm Th (ng)	Th/U	Date (Ma)	2 σ \pm date (Ma)
Undeformed									
<i>Single plate</i>									
EXP_1_H1	0.271	0.000	0.185	0.003	0.010	0.000	0.055	261	7
EXP_1_H2	0.172	0.003	0.129	0.002	0.014	0.000	0.107	235	10
EXP_1_H3	0.060	0.001	0.037	0.001	0.003	0.000	0.088	287	13
EXP_1_H4	0.018	0.000	0.015	0.000	0.003	0.000	0.191	207	10
EXP_1_H5	0.336	0.005	0.252	0.004	0.057	0.001	0.232	231	9
EXP_1_H6	0.047	0.001	0.027	0.000	0.010	0.000	0.389	284	10
EXP_2_H1	0.011	0.000	0.010	0.000	0.004	0.000	0.406	176	6
EXP_2_H2	0.002	0.000	0.002	0.000	0.001	0.000	0.541	166	11
EXP_2_H3*	0.002	0.000	0.001	0.000	0.001	0.000	0.651	280	27
EXP_2_H4	0.036	0.000	0.034	0.001	0.007	0.000	0.201	183	5
EXP_2_H5	0.017	0.000	0.011	0.000	0.003	0.000	0.265	255	10
EXP_2_H6*	0.037	0.000	0.009	0.000	0.008	0.000	0.881	603	21
EXP_2_H7	0.038	0.000	0.027	0.000	0.004	0.000	0.168	251	9
EXP_2_H8	0.191	0.002	0.130	0.002	0.014	0.000	0.108	259	9
EXP_2_H9	0.038	0.000	0.023	0.000	0.006	0.000	0.264	286	10
EXP_2_H10	0.758	0.008	0.555	0.0079	0.049	0.001	0.090	243	9
<i>Homogenized (polycrystalline)</i>									
22_H1	0.291	0.001	0.234	0.003	0.031	0.000	0.137	219	6
22_H2	0.373	0.001	0.275	0.004	0.029	0.000	0.106	240	7
22_H3	0.368	0.001	0.367	0.005	0.089	0.001	0.247	173	5
23_H1	0.332	0.001	0.353	0.005	0.094	0.001	0.272	162	4
23_H2	0.301	0.001	0.296	0.004	0.087	0.001	0.302	174	5
23_H3	0.269	0.001	0.238	0.004	0.055	0.001	0.235	195	5
<i>Undegassed aliquots (no He extraction)</i>									
22_H4	-	-	0.244	0.004	0.030	0.000	0.125	-	-
22_H5	-	-	0.337	0.005	0.035	0.001	0.108	-	-
22_H6	-	-	0.374	0.005	0.060	0.001	0.163	-	-
23_H4	-	-	0.312	0.005	0.065	0.001	0.214	-	-
23_H5	-	-	0.345	0.005	0.083	0.001	0.245	-	-
23_H6	-	-	0.305	0.004	0.057	0.001	0.190	-	-
Experiment run products									
<i>Fault gouge – continuous slip</i>									
22_G_H1	0.286	0.003	0.273	0.004	0.072	0.001	0.272	180	6
22_G_H2	0.381	0.004	0.383	0.006	0.114	0.002	0.306	170	6
22_G_H3	0.217	0.002	0.218	0.003	0.069	0.001	0.325	169	6
<i>Fault gouge – interrupted slip</i>									
23_G_H1	0.139	0.002	0.162	0.002	0.102	0.002	0.648	137	5
23_G_H2	0.074	0.001	0.076	0.001	0.046	0.001	0.630	157	5
23_G_H3	0.426	0.005	0.437	0.006	0.152	0.002	0.357	165	6
<i>Fault mirror – continuous slip</i>									
22_S_H1	0.110	0.001	0.312	0.005	0.071	0.001	0.232	62	2
22_S_H2*	0.030	0.000	0.039	0.001	0.039	0.001	1.039	116	4
22_S_H3	0.168	0.002	0.473	0.007	0.239	0.003	0.518	59	2
<i>Fault mirror – interrupted slip</i>									
23_S_H1	0.013	0.000	0.017	0.000	0.013	0.000	0.766	113	4
23_S_H2	0.011	0.000	0.014	0.000	0.010	0.000	0.719	117	4
23_S_H3*	0.023	0.000	0.040	0.001	0.039	0.001	1.010	86	3

*Aliquots excluded from the discussion. Please see text in Data Repository section 4 above for more details.

Table DR3: Hematite He loss assessment

	Date (Ma)	1 σ Ma	Δ date (Ma)	Error, δ (Ma)	% He loss	Error % He loss
Continuous slip experiment						
Undeformed homogenized						
22_H1	219	3				
22_H2	240	3				
22_H3	173	2				
mean/std dev	211	34				
Fault mirror						
22_S_H1	62	1	149	34	71	12
22_S_H3	59	1	152	34	72	12
mean			151	2	71	1
Gouge						
22_G_H1	180	3	31	34	15	2
22_G_H2	170	3	41	34	20	3
22_G_H3	169	3	42	34	20	3
mean			38	6	18	3
Interrupted slip experiment						
Undeformed homogenized						
23_H1	162	2.2				
23_H2	174	2.3				
23_H3	195	2.7				
mean/std dev	177	16.8				
Fault mirror						
23_S_H1	113	2.1	64	17	36	3
23_S_H2	117	2.1	59	17	34	3
mean			62	3	35	2
Gouge						
23_G_H1	137	2.3	39	17	22	2
23_G_H2	157	2.7	20	17	11	1
23_G_H3	165	2.8	12	17	7	1
mean			24	14	13	8

Table DR4: Frictional generated heat calculations parameters

	Symbol	Units	Comments	Reference
<i>Hematite coefficient of friction</i>	μ	0.28	Mean value during experiments	This study
<i>Normal load</i>	σ_n	8.5 MPa	Load used in experiments	This study
<i>Hematite density</i>	ρ	5300 Kg/m ³	Literature	(Nesse, 2012)
<i>Heat capacity</i>	c	137.67 J/kg K	Literature	(Chase, 1983)
<i>Slip velocity</i>	V	0.25 m/s	Mean slip velocity during experiments	This study
<i>Hematite thermal conductivity</i>	k	11.3 W/mK	Literature	(Horai, 1971)
<i>Hematite thermal diffusivity</i>	α	1.55x10 ⁻⁵ m ² /s	$\alpha = k/(\rho c)$	
<i>Hematite indentation hardness</i>	H	2.7 GPa	Literature	(Chicot et al., 2011)

Table DR5: Friction-generated heat calculations

<i>Average fault surface temperature rise (AFST)</i>			
AFST after 1 cycle °C	AFST after 40 cycles °C		
64	305		

<i>Asperity flash heating (AFT)</i>			
Asperity diameter (μm)	Peclet number	AFT- AFST (°C)	Asperity lifetime (s)
5	0.020	16	2.0E-05
10	0.040	33	4.0E-05
20	0.081	65	8.0E-05
30	0.121	97	1.2E-04
40	0.161	129	1.6E-04
50	0.202	161	2.0E-04
100	0.403	315	4.0E-04
150	0.605	462	6.0E-04
200	0.806	603	8.0E-04
250	1.008	738	1.0E-03
300	1.210	865	1.2E-03
350	1.411	986	1.4E-03
400	1.613	1101	1.6E-03
450	1.815	1209	1.8E-03
500	2.016	1310	2.0E-03
550	2.218	1404	2.2E-03
600	2.419	1492	2.4E-03

FIGURES

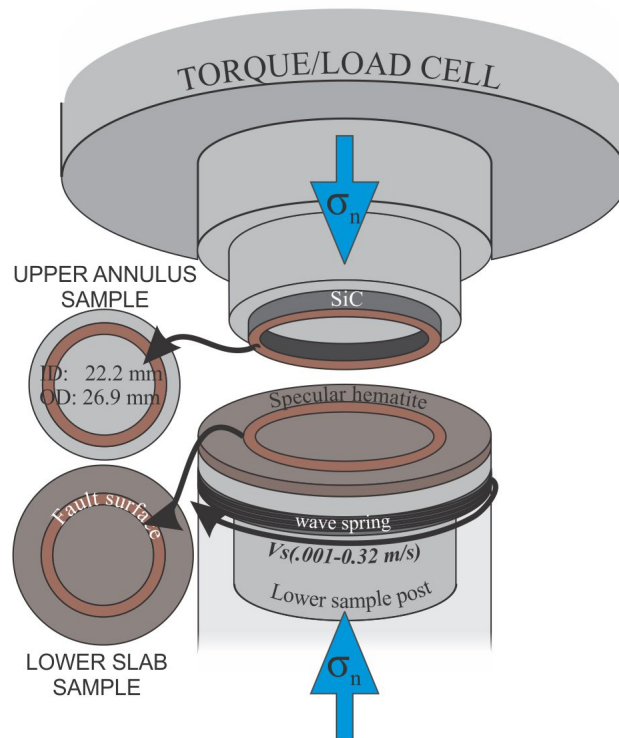


Figure DR1: Schematic of Instron 1 atm rotary shear apparatus showing the load/torque cell and sample grip assembly. Modified from Kohli et al. (2011).

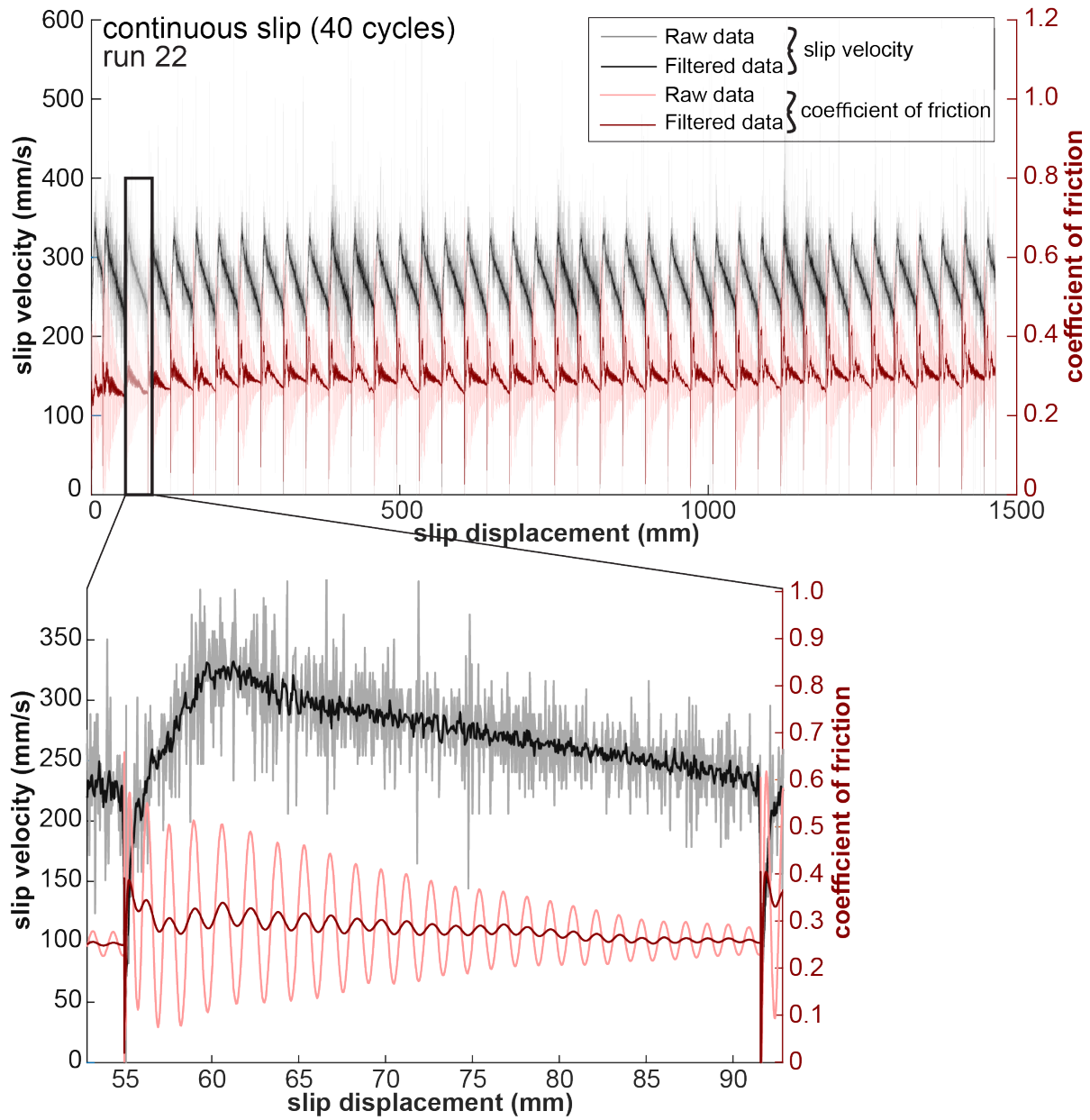


Figure DR2: Data from the continuous slip experiment, run 22. Raw and filtered slip velocity (thin and thick black lines, respectively) and coefficient of friction (thin and thick red lines) data, recorded at 5 kHz, are plotted as a function of slip displacement. Bottom panel is an enlargement of the third cycle.

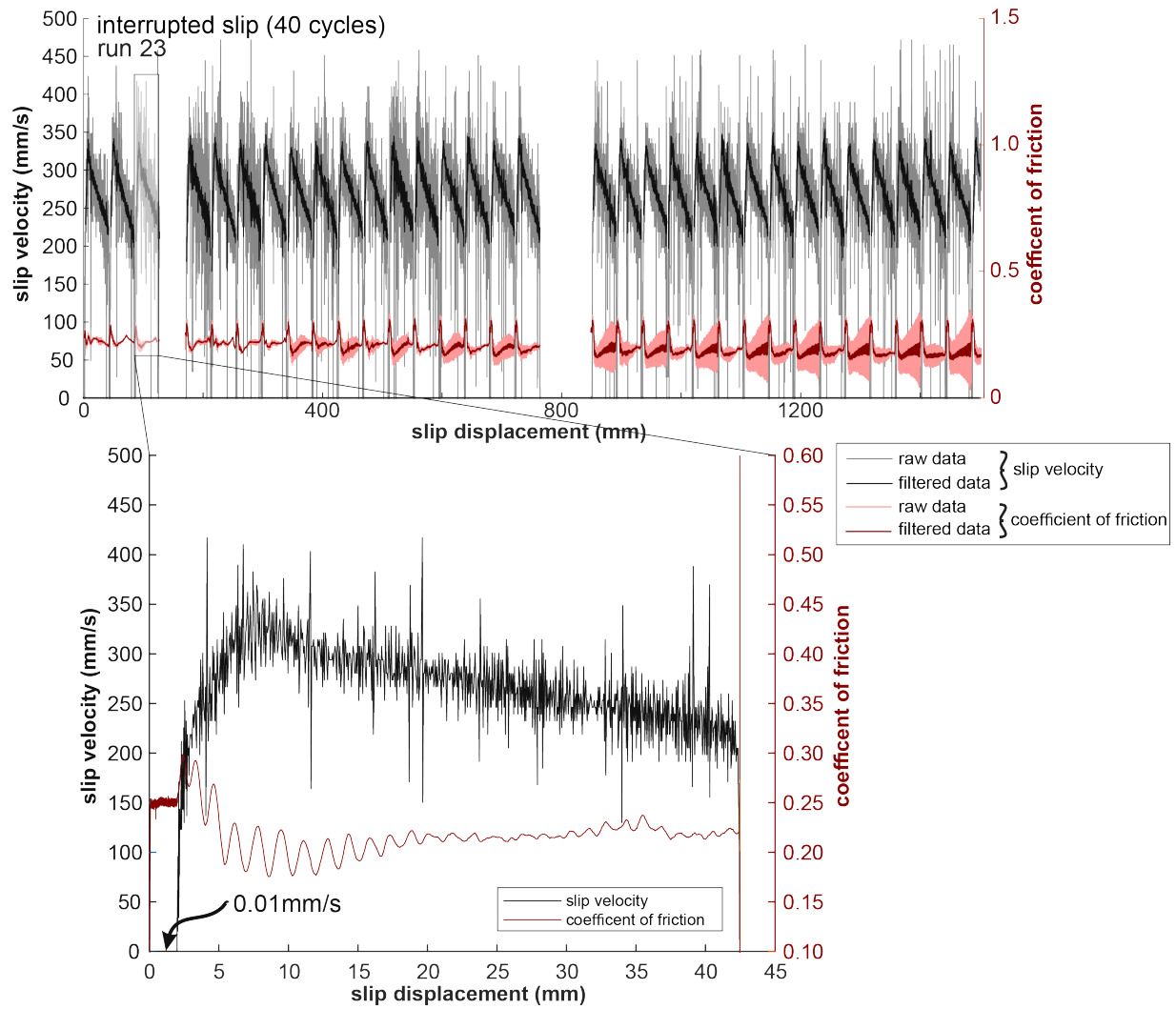


Figure DR3: Data from the interrupted slip experiment. Raw and filtered slip velocity (thin and thick black lines) and coefficient of friction (thin and thick redlines) data, recorded at 5 kHz, are plotted as a function of slip displacement. Insert is an enlargement of the third cycle, but ease of reading, only filtered slip velocity and coefficient of friction data are shown.

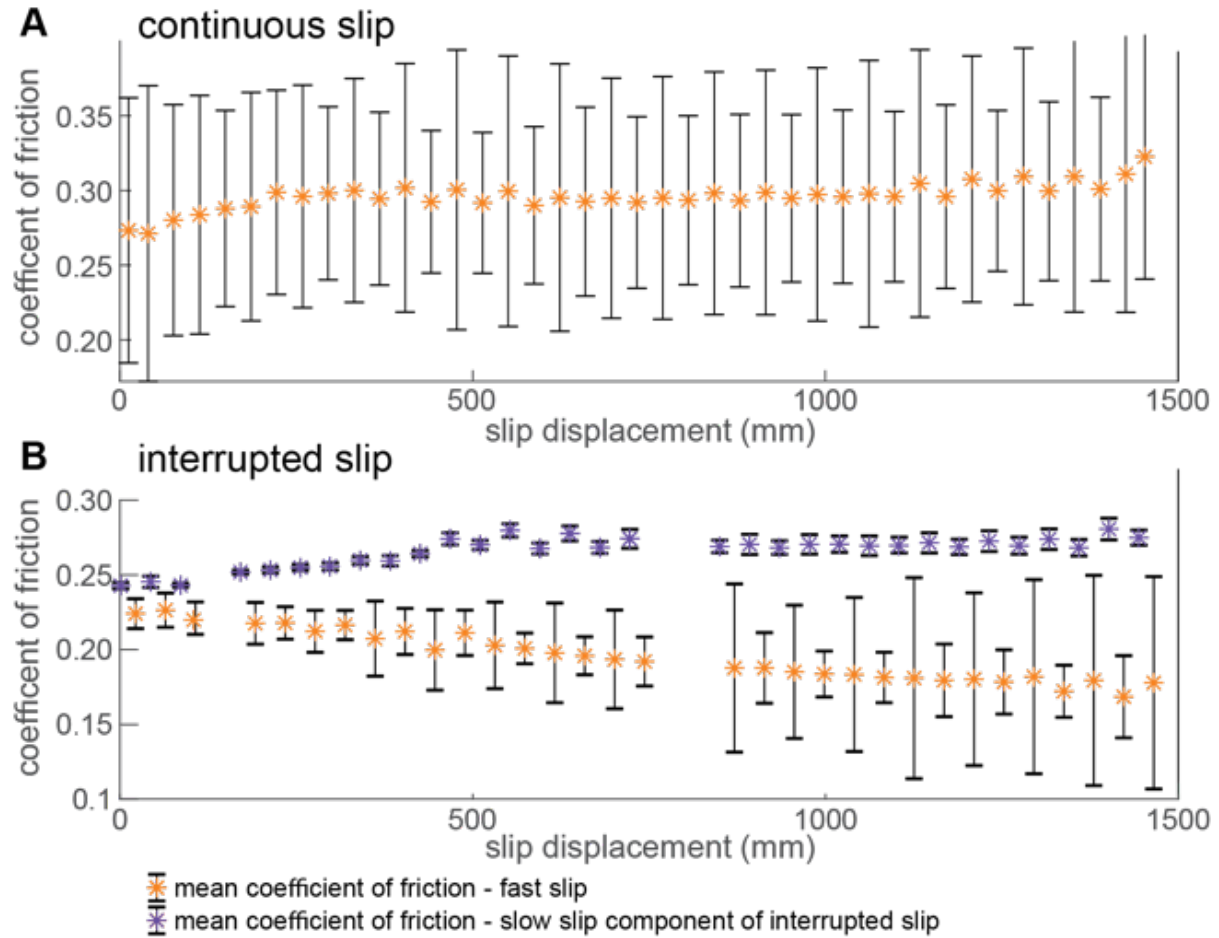


Figure DR4: Summary of mechanical data from continuous slip (A) and interrupted slip (B) experiments. Each plot shows the mean coefficient of friction for each cycle (orange). For the interrupted slip experiment, the mean coefficient of friction was calculated for the slow slip (0.01 mm s^{-1} ; in purple) and fast slip (320 m s^{-1} ; in orange) components of each cycle.

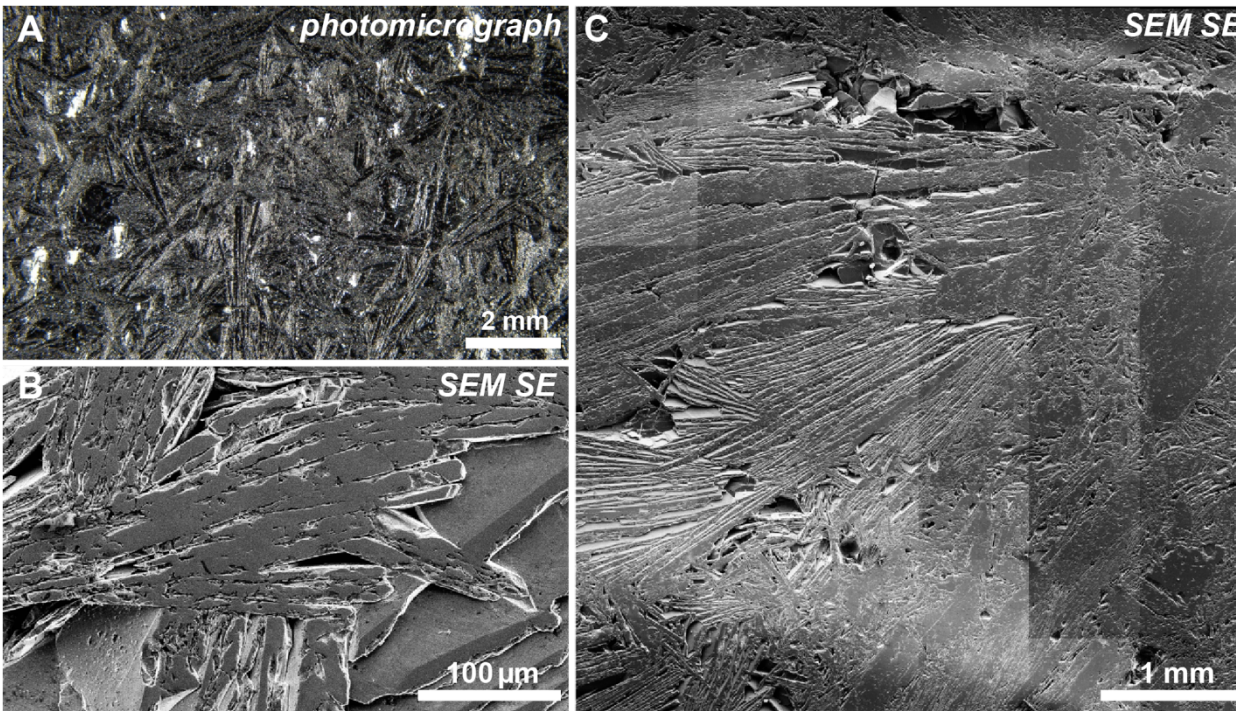


Figure DR5: Photomicrograph (A), example scanning electron microscopy secondary election (SEM SE) image (B), and SEM SE image montage (C) of the polycrystalline, specular hematite starting material.

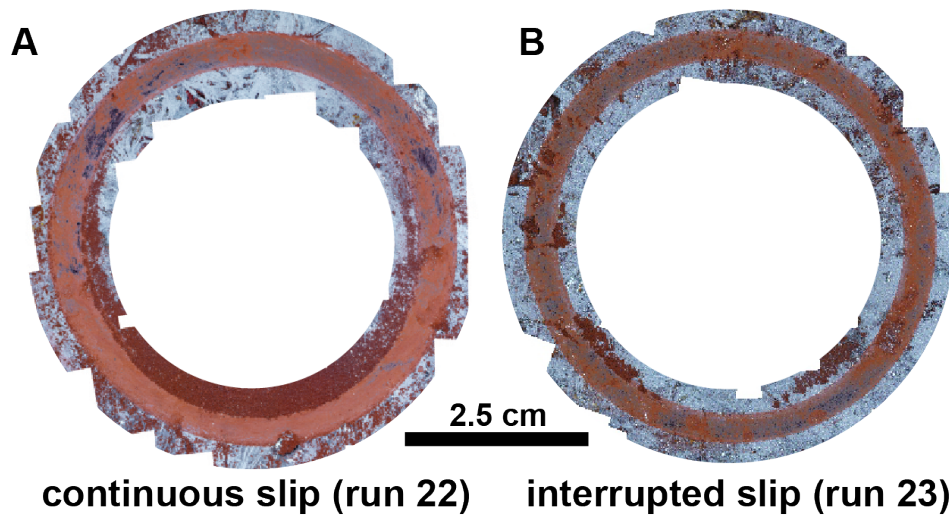


Figure DR6: Composite photomicrographs of the hematite lower slab sample at the end of each experiment.

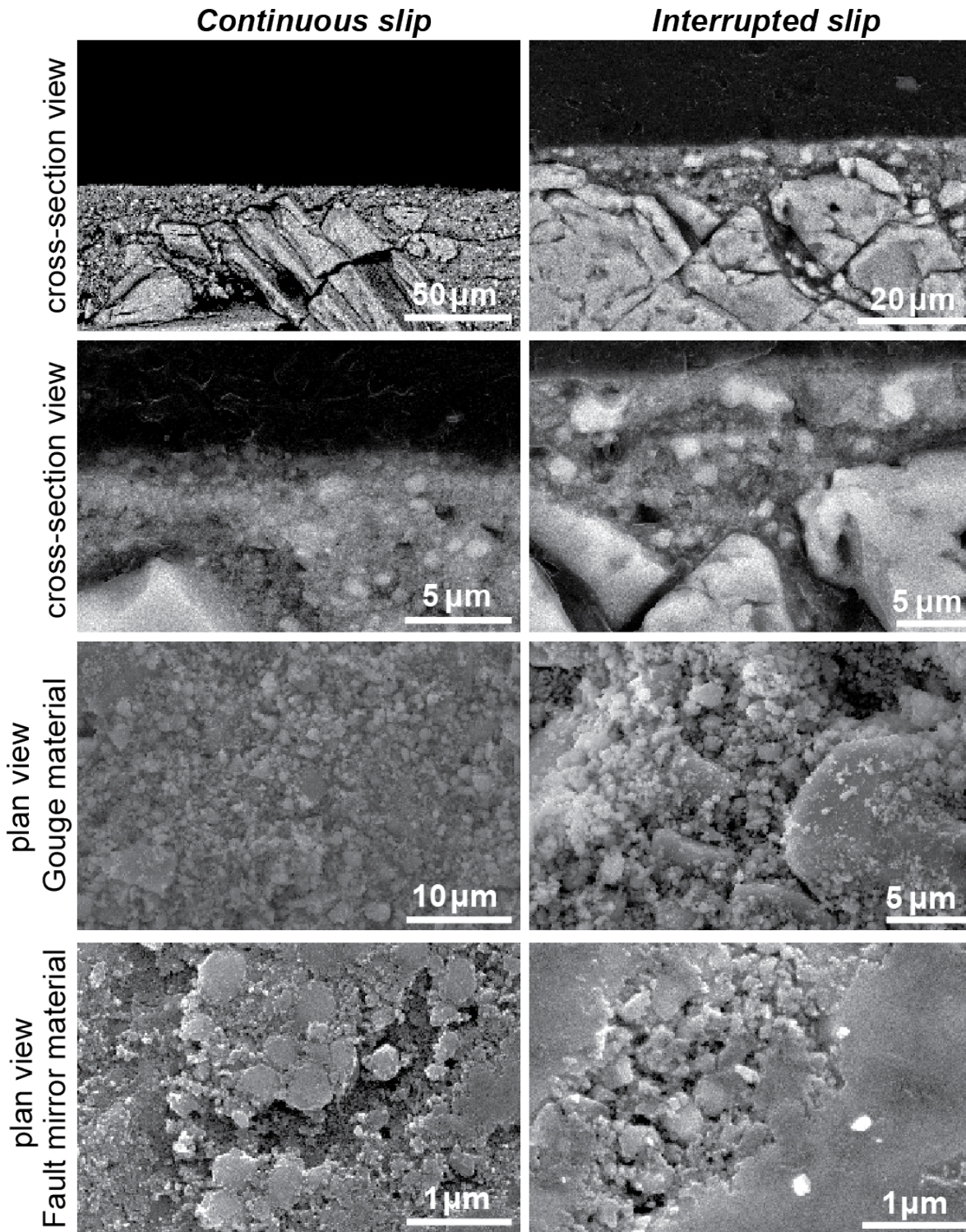


Figure DR7: Representative SEM SE images of the experimentally-produced fault surfaces from the lower hematite slab. Images are taken in cross-sectional and plan views.

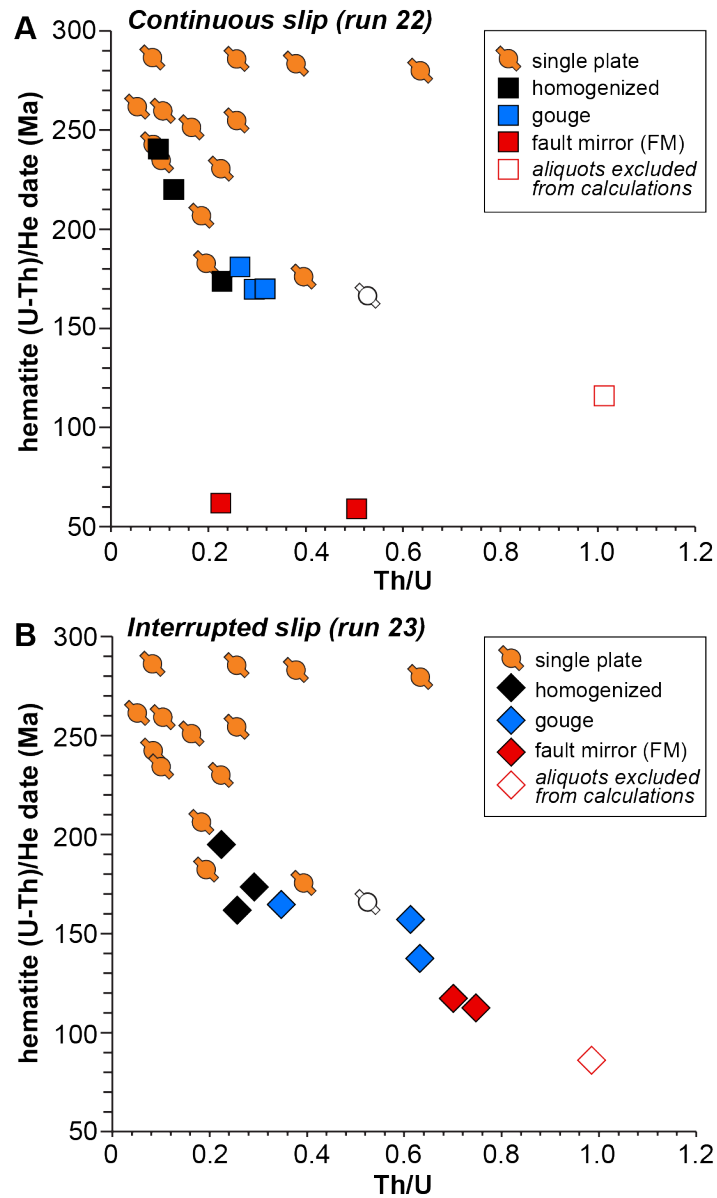


Figure DR8: Th/U ratio as a function of hematite (U-Th)/He date in Ma plot for fault mirror (FM, red), gouge (blue), undeformed homogenized aliquots (black), and undeformed single plates (orange) from continuous slip (A) and interrupted slip (B) experiments. White filled symbols are aliquots with elevated Th/U ratios that are excluded from the discussion (see prior description in Data Repository section 4).

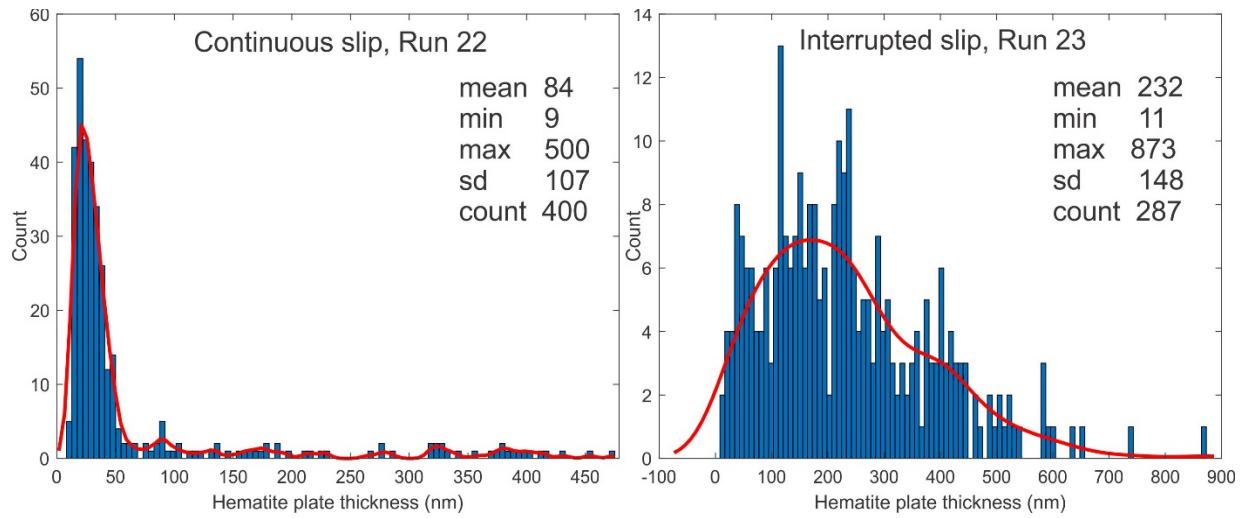


Figure DR9: Plate thickness distribution histograms and statistics for the experimentally-produced fault mirror (FM) material in continuous and interrupted slip experiments. Grain size analysis was carried out using SEM SE images and ImageJ software. sd = standard deviation.

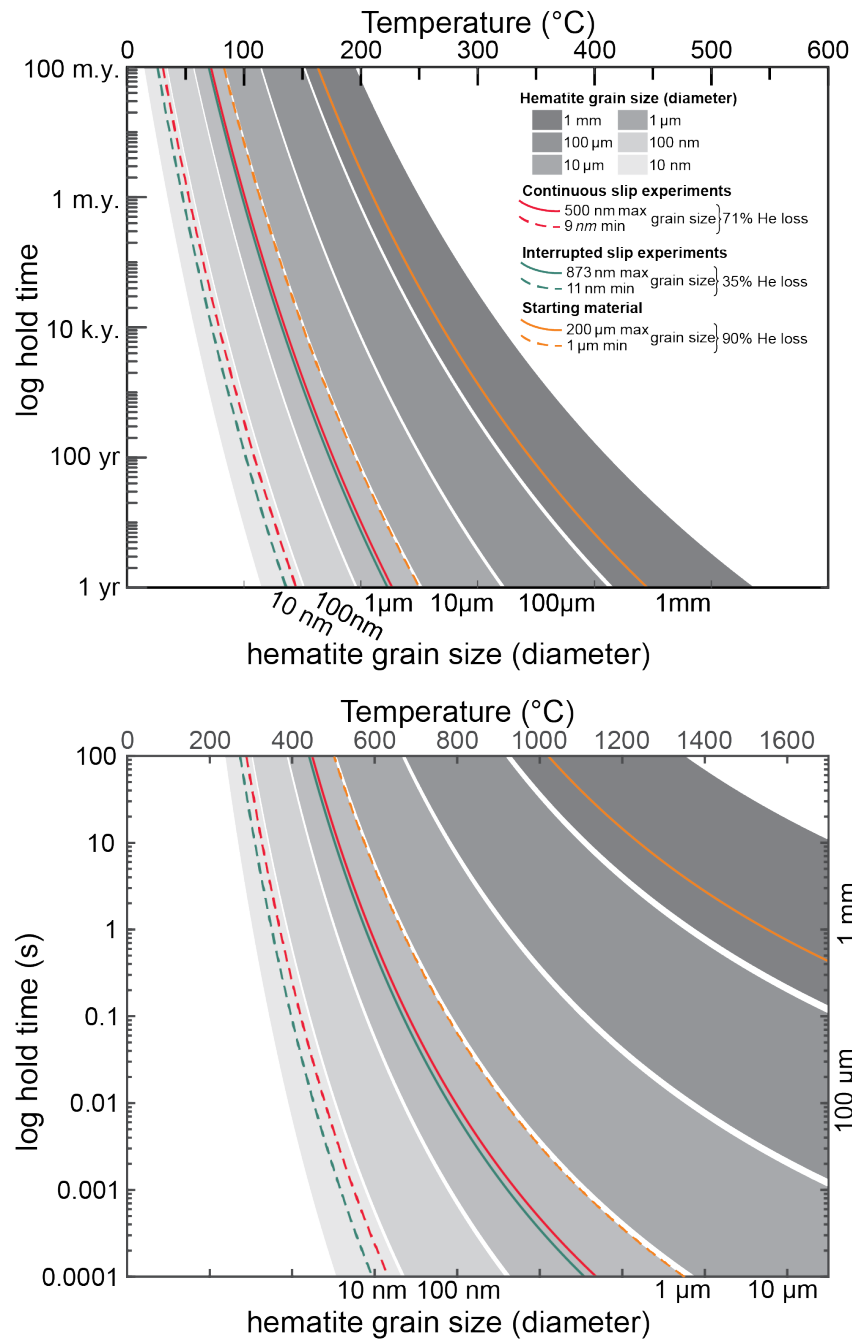


Figure DR10: Estimated temperature rise on experimental fault surfaces via calculated hematite He fractional loss contours for continuous slip experiment (red curves), interrupted slip experiment (green curves), and starting material (orange curves), applying maximum (solid line) and minimum (dashed line) hematite grain size (plate thickness) measured from SEM images. Shaded areas represent the closure temperatures (envelope between 10% and 90% fractional He loss) for different hematite plate thicknesses or particle diameters. Calculations assume a square-pulse heating event and use hematite He diffusion parameters from Farley (2018). Top diagram: time in years. Bottom diagram: time in seconds.